Heterogeneous Thin-Film Lithium Niobate Integrated Photonics for Electrooptics and Nonlinear Optics

Ashutosh Rao, *Student Member, IEEE*, and Sasan Fathpour, *Senior Member, IEEE*

(Invited Paper)

***Abstract*—Ion-sliced thin-film lithium niobate (LN) compact waveguide technology has facilitated the resurgence of integrated photonics based on the material. The thin-film waveguides offer over an order of magnitude improvement in optical confinement and bending radius compared to conventional LN waveguides. The thin-film technology can also be implemented on versatile silicon substrates. Harnessing the improved confinement, a variety of miniaturized and efficient photonic devices has been realized. The state of the art of thin-film LN integrated photonics is reviewed, focusing on heterogeneous integration, electrooptic modulation, and nonlinear frequency conversion. The potential applications and associated challenges of next-generation LN-based integrated photonics are discussed.**

***Index Terms*—Lithium niobate, thin film, nanophotonics, electrooptic modulation, electrooptic devices, nonlinear optics, nonlinear optical devices, optical waveguides, microwave photonics, optical fiber communication, photonic integrated circuits, silicon photonics, photonics.**

I. Introduction

LITHIUM niobate (LN) has enjoyed widespread commercial success through its applications in telecommunications [1] and nonlinear optics [2], [3]. Modulators and switches, which benefit from the strong electrooptic (EO) effect in LN, have been vital to the development of optical telecommunications [4]–[9]. In addition, periodically-poled LN (PPLN), which relies on ferroelectric domain reversal and the material's strong second-order nonlinear effect, has been central to the development of numerous nonlinear devices, such as optical frequency converters and parametric oscillators [10]–[15]. LN has been used in many other applications as well, for example, as Q-switches for lasers [16]–[18], and as entangled photon-pair sources for quantum optics applications [19], [20].

Fig. 1. A fully-packaged commercial LN EO Mach-Zehnder modulator. The total packaged length is ∼13 cm, and the internal LN chip is ∼9 cm long. The long length is a consequence of high voltage-length product, and high bending radius; both of these shortcomings of conventional LN waveguides are addressed through the presented thin-film platform.

However, conventional LN devices usually have large on-chip footprints. For example, a typical commercial-off-the-shelf (COTS) LN EO modulator is 5 to 10 cm long (Fig. 1). Recently, there has been a push towards miniaturizing LN-based photonic devices, with the goal of forming complex and compact integrated circuits. The desired reduction in size is usually accompanied by an increase in efficiency (specific to each device), as discussed later. Furthermore, monolithic integration of these compact LN devices on silicon substrates enables potential compatibility with silicon photonics and back-end-of-line (BEOL) foundry fabrication.

These objectives have been pursued using thin-film LN integrated photonics, the focus of this review article. Section II briefly introduces the relevant material and optical properties of LN. Section III describes the modernization of LN integrated photonics from large diffused waveguides to submicron thin-films that are compatible with current trends in integrated photonics, particularly on silicon substrates. The heterogeneous integration of thin-film LN with a variety of other optical materials is reviewed in Section IV. Section V discusses thin-film LN EO and nonlinear optical devices. Finally, we conclude with an outlook on the potential future uses of thin-film LN and a summary on the state of the art.

II. Lithium Niobate

A. Physical Properties of Lithium Niobate

Lithium niobate is a synthetic dielectric that exhibits ferroelectricity (spontaneous electric polarization) below its Curie

Manuscript received January 31, 2018; revised April 23, 2018; accepted May 7, 2018. Date of publication May 17, 2018; date of current version June 11, 2018. This work was supported in part by the U.S. Office of Naval Research Young Investigator Program, in part by the Defense Advanced Research Projects Agency DODOS program, in part by the Department of Energy, in part by the National Science Foundation, in part by the National Aeronautics and Space Administration and in part by the Harris Corporation. (*Corresponding author: Sasan Fathpour*.)

A. Rao is with the Center for Research and Education in Optics and Lasers, The College of Optics and Photonics, University of Central Florida, Orlando, FL 32816 USA (e-mail: ashutoshrao@knights.ucf.edu).

S. Fathpour is with the Center for Research and Education in Optics and Lasers, The College of Optics and Photonics, Department of Electrical and Computer Engineering, University of Central Florida, Orlando, FL 32816 USA (e-mail: fathpour@creol.ucf.edu).

Color versions of one or more of the figures in this paper are available online at http://ieeexplore.ieee.org.

Digital Object Identifier 10.1109/JSTQE.2018.2836939

1077-260X © 2018 IEEE. Personal use is permitted, but republication/redistribution requires IEEE permission.
See http://www.ieee.org/publications_standards/publications/rights/index.html for more information.

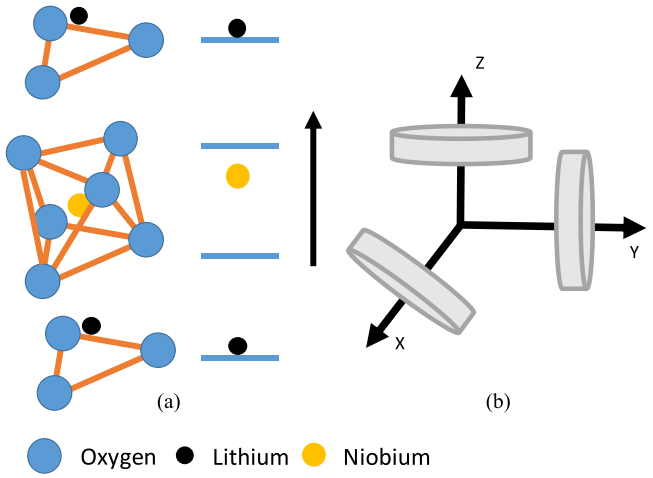

Fig. 2. (a) Crystal structure of ferroelectric lithium niobate. The blue spheres represent oxygen atoms, which form planes normal to the crystal c-axis. The positions of the niobium (gold colored spheres) and lithium (black colored spheres) ions dictate the ferroelectric domain orientation (upwards here). The periodic vacancy is visible between the upper lithium and niobium atoms. After [31]. (b) X, Y and Z-cuts of LN wafers are important for optical applications.

temperature. The use of the Czochralski technique [21] for the growth of ferroelectrics [22], and the synthesis of single crystals of LN and their associated material properties, were studied in detail in the 1960s, particularly in Bell Laboratories [23]–[29]. By the late 1970s, research on LN had caught up with barium titanate, a longstanding popular choice for the study of fundamental science and applications in ABO_3-type ferroelectrics. LN is primarily grown in two variants – congruent (lithium deficient), and stoichiometric [30]. Congruent LN has been widely used in optical applications due to its low absorption and high homogeneity. Nonetheless, stoichiometric LN has been pursued more recently due to its reduced lattice defects and lower localized field distortions. A notable consequence of the improved stoichiometry is a strong reduction in the internal coercive field.

The ferroelectric phase of LN is a trigonal crystal (Fig. 2(a)) belonging to the $3m$ point group and the $R3c$ space group [25], [31]. LN has been doped with many different materials (e.g., magnesium, zinc, indium, zirconium, hafnium, and tin) to ameliorate its susceptibility to optical damage [32]–[38].

LN has been widely studied for its pronounced piezoelectric, pyroelectric, photoelastic, nonlinear optical, and electrooptical properties. The tensors describing these properties are commonly given with respect to the orthohexagonal axes of LN. The material is anisotropic, and its low-frequency relative permittivity is given in Table I for both unclamped (zero mechanical stress) and clamped (zero mechanical strain) crystals. Other material properties are also summarized in Table I. In addition, the coefficients to a three-oscillator Sellmeier equation [39],

$$n = \begin{bmatrix} n_o & 0 & 0 \\ 0 & n_o & 0 \\ 0 & 0 & n_e \end{bmatrix}, \tag{1a}$$

$$n_{e/o}^2 = 1 + \frac{A\lambda^2}{\lambda^2 - B} + \frac{C\lambda^2}{\lambda^2 - D} + \frac{E\lambda^2}{\lambda^2 - F} \tag{1b}$$

TABLE I
PHYSICAL PROPERTIES OF CONGRUENTLY GROWN LN [3], [31]

Property	Value
Crystal structure	Trigonal
Point group	$3m$
Space group	$R3c$
Coefficient of thermal expansion (300 K)	
α_a (K^{-1})	14.1
α_c (K^{-1})	4.1
Melting point (°C)	1240
Curie Temperature (°C)	1140
Spontaneous polarization ($\mu C/cm^2$)	71
Hardness (mohs)	5
Low-frequency relative permittivity (unclamped)	$\varepsilon_{xx} = \varepsilon_{yy} = 84.1$, $\varepsilon_{zz} = 28.1$
Low-frequency relative permittivity (clamped)	$\varepsilon_{xx} = \varepsilon_{yy} = 46.5$, $\varepsilon_{zz} = 27.3$
Electrooptic tensor r (pm/V) (all coefficients not listed are zero)	$r_{33} = 30.8$, $r_{13} = r_{23} = 8.6$, $r_{22} = -r_{12} = -r_{61} = 3.4$, $r_{51} = r_{42} = 28$
Nonlinear tensor d (pm/V) (all coefficients not listed are zero)	$d_{33} = 30$, $d_{31} = d_{32} = d_{24} = d_{15} = 5.9$, $d_{22} = -d_{21} = -d_{16} = 3.0$

TABLE II
THREE-OSCILLATOR SELLMEIER COEFFICIENTS FOR CONGRUENTLY GROWN LN [40]

Coefficient	n_e	n_o
A	2.9804	2.6734
B	0.02047	0.01764
C	0.5981	1.2290
D	0.0666	0.05914
E	8.9543	12.614
F	416.08	474.6

for the ordinary and extraordinary refractive indices of congruently grown LN at optical frequencies are listed in Table II [40].

B. Pockel's Effect

The EO coefficients of LN are large, and have therefore been used to form optical modulators in both bulk crystals and integrated waveguides. The linear EO effect, also called the Pockel's effect [41], describes the change in the refractive index of a material upon the application of a direct-current (DC) or radio-frequency (RF) electric field. The refractive index change is proportional to the applied electric field. The EO effect is quantified as

$$\Delta\left(1/n_{ij}^2\right) = \sum_k z_{ijk} E_k;\ i, j, k = x, y, z, \tag{2}$$

where the coefficients z_{ijk} form the third-rank Pockel's tensor, n_{ij} is the (i, j) element of the second-order refractive index tensor, and E_k is the k^{th} Cartesian component of the external electric field. Using symmetry arguments, the third-rank Pockel's tensor is commonly contracted to a 6×3 matrix, r, called the EO matrix [3]. The r matrix coefficients for LN are listed in Table I.

When an external electric field, E, is applied along the crystalline c-axis (or the z axis) of LN, the material refractive index is perturbed as $\Delta n = -n_e^3 r_{33} E/2$ [42]. Then, the effective refractive index, n_{eff}, of a guided mode propagating perpendicular to and polarized along the c-axis is accordingly modulated, within a first-order Taylor approximation, as

$$n_{\text{eff}}(E) \approx n_{\text{eff}} - n_e^4 r_{33} E/(2n_{\text{eff}}). \tag{3}$$

This refractive index modification is at the core of LN EO modulators. It is noted that in conventional EO modulator models, it is common and fair to assume $n_{\text{eff}} \approx n_e$ in (3) [42]. However, in modern compact devices with much higher core-clad index contrast (e.g., LN of $\sim$2.1 vs. SiO_2 of $\sim$1.5), it is important to differentiate between the two indices. An electromagnetic wave of wavelength λ, traveling perpendicular to and polarized along the z-axis, accumulates a change in optical phase due to the electric field along the z-axis,

$$\Delta\Phi(E) = \frac{2\pi L\left[n_{\text{eff}}(E(t)) - n_{\text{eff}}\right]}{\lambda} = -\frac{\pi L n_e^4 r_{33} E(t)}{\lambda n_{\text{eff}}}, \tag{4}$$

where L is the length traversed, and the variation of E with time leads to phase modulation. The interference of two such phase-modulated waves leads to intensity modulation. The state of the art of thin-film LN EO modulators is reviewed in Section IV.

C. Second-Order Optical Nonlinearity

LN has been widely used for second-order nonlinear optics because of its high nonlinear coefficients, low optical absorption, wide optical transmission window, and ferroelectric nature, which permits the engineering of efficient nonlinear interactions via ferroelectric domain reversal (often called periodic poling). Second-order nonlinear optics, or three-wave mixing, addresses nonlinear interactions between three photons that are mediated by the second-order nonlinear susceptibility, $\chi^{(2)}$, a third-rank tensor. Three-wave mixing processes include sum, difference, and second harmonic generation (SFG, DFG, and SHG), optical parametric amplification and oscillation (OPA and OPO), and spontaneous parametric down-conversion (SPDC).

The second-order nonlinear polarization, $P^{(2)}$, is the driving force for $\chi^{(2)}$ interactions. $P^{(2)}$ for SFG is given by [3]

$$P_i^{(2)}(\omega_3) = \varepsilon_0 \sum_j \sum_k \chi_{ijk}^{(2)}(\omega_3;\omega_1,\omega_2) E_j(\omega_1) E_k(\omega_2) e^{i\Delta\beta_{ijk}}, \tag{5}$$

where i, j, k refer to the Cartesian axes, $\omega_3 = \omega_1 + \omega_2$ is the sum of the two incident angular frequencies ω_1 and ω_2, $E_j(\omega_m)$ is the j^{th} component of the interacting electric fields at frequency $\omega_m >$, $\Delta\beta_{ijk}$ is the phase difference between the interacting waves, and $\chi_{ijk}^{(2)}$ is the $(i,j,k)^{th}$ element of the $\chi^{(2)}$ tensor. Depending on the incident polarizations, only certain elements of $\chi^{(2)}$ contribute to the interaction. Following symmetry arguments, $\chi^{(2)}$ is often contracted to the nonlinear tensor d, expressed by a 3×6 matrix. The d tensor for LN is listed in Table I. The null elements are determined by the crystal symmetries of LN. Efficient three-wave interactions require phase-matching (PM), a compensation of momentum mismatch between the interacting waves. This implies that $\Delta\beta_{ijk}$ is required to be either zero, or compensated for by a spatial modulation in the product of the nonlinear susceptibility and the electric field modes. A few significant approaches for PM and efficient nonlinear frequency conversion in thin-film LN are reviewed in Section IV.

III. Modernization of Lithium Niobate Photonics

The success of LN for photonics applications was driven, in part, by stripe waveguide optimization which led to salutary low propagation and coupling loss, along with other application-specific improvements [43]–[47]. Traditionally, the in-diffusion of titanium around 1000 °C has been used to form stripe waveguides (Ti:LN) in bulk LN wafers [43]–[45]. Ti:LN waveguides were widely studied and improved for commercial applications such as EO modulators. Titanium diffusion increases both the ordinary and the extraordinary indices of refraction. Therefore, both transverse-electric (TE) and transverse-magnetic (TM) modes can be guided, depending on the characteristics of the Ti diffusion. A different diffused waveguiding approach uses proton exchange (PE) [48], [49], where the LN is locally exposed to a proton-rich acid bath, typically at low temperatures (up to 300 °C). Protons replace Li ions through diffusion to form a series of distinct graded phases with varying ratios of protons to Li ions. The extraordinary index increases in the PE layers, usually accompanied by local refractive index instability, increased optical scattering, and degraded EO and nonlinear coefficients, while the ordinary index remains unaffected. PE is followed by a controlled high-temperature processing step, forming annealed proton exchanged (APE) waveguides [50], to diminish some of the aforementioned undesired effects of PE. Finally, the APE process can be followed by a reverse proton exchange (RPE) step [51]. RPE uses a controlled and limited local reversal of the first PE step by immersion in a lithium-rich melt, leading to an enhanced nonlinear mode overlap for nonlinear applications.

While APE waveguides offer sufficient EO coefficient recovery for EO applications, and RPE waveguides resolve the insufficient nonlinear mode overlap of APE waveguides for nonlinear optical applications, alternative solutions have been explored for further improvement in the performance of devices through waveguide optimization. For example, a combination of dry etching and Ti diffusion can be used to form wide etched ridge Ti:LN waveguides in single crystal bulk LN substrates for EO modulators. Ridge Ti:LN waveguides have been important in advancing EO modulator technology by enabling drive voltage reduction, to a certain extent, and increased RF modulation bandwidths [52]. Nonetheless, the optical confinement offered by such schemes remains insufficient to meet the demands of modern integrated photonics – small device footprints, tight bending radii, low power consumption, etc.

Improved optical confinement would offer ample improvements from a single-device perspective as well. Electrodes could be brought closer to increase the electric field per volt applied to the electrodes, thereby enhancing EO modulation efficiency (Fig. 3(a)–3(c)). Nonlinear optical interaction efficiencies would drastically increase because of the stronger nonlinear interaction and overlap (Fig. 3(d)–3(g)). The increase in efficiencies

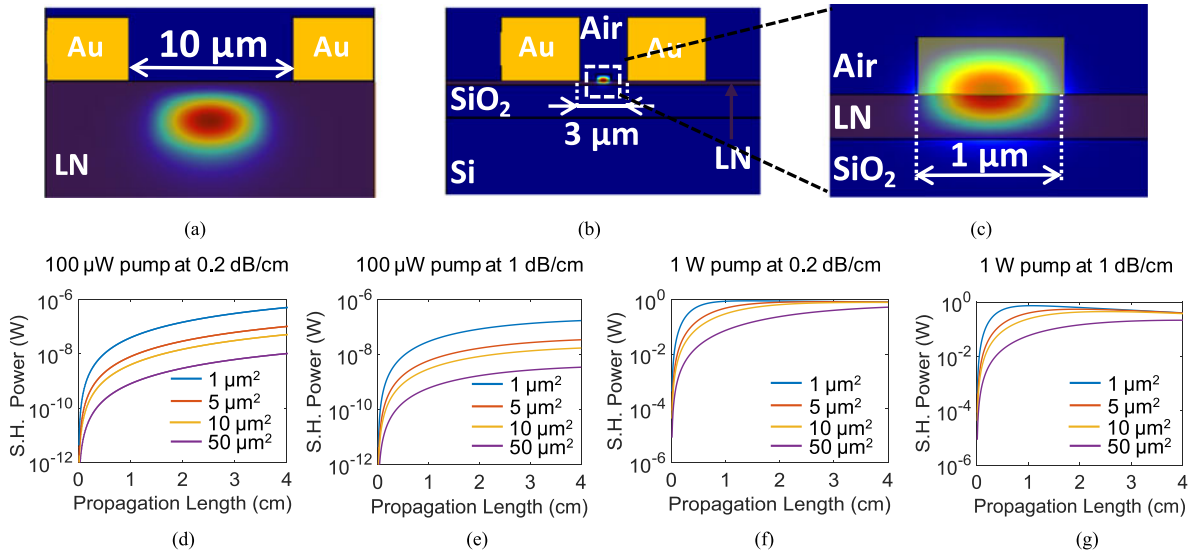

Fig. 3. (a) Optical mode of a typical titanium-diffused LN waveguide at 1550 nm. The low index contrast offered by the diffusion limits the minimum size of the waveguide mode, and the gap between the two gold electrodes. A smaller gap results in significant electrode metal-induced optical loss. (b) In contrast, thin-film LN waveguides offer submicrometer optical confinement, enabling electrode gap reduction by over a factor of 3 compared to (a). (a) and (b) are drawn to scale to emphasize the increase in optical confinement. (c) Magnified image of the optical mode in (b). The LN thin-film is 300 nm thick, and the 400-nm-tall rib, which can be a heterogeneously integrated material, or etched LN itself, has an index of 2.2. (d)–(g) Effect of increased optical confinement (shown in the legends), on second-harmonic generation efficiency with different pump powers and propagation losses, plotted vs. propagation length. The smaller waveguides offer higher nonlinear frequency conversion, even at losses of 1 dB/cm.

would be accompanied by a reduction in device size and both electrical and optical power consumption. Also, the success of silicon photonics has led to integrability on silicon substrates being an important concern as well.

All of these considerations can be met in photonic platforms that are based on thin films of LN in order to fabricate tightly-confined waveguides [53]–[57]. The first demonstration of monolithic integration of LN thin films on silicon substrates, as well as waveguides and EO modulators on the new platform, was reported by researchers at CREOL in 2013 [54]. As summarized in Fig. 4, helium ions are implanted into a donor LN wafer, which is bonded to a layer of SiO_2 on a Si handle wafer. The donor-handle wafer combination is then annealed to slice the donor wafer close to the implanted region, in order to form a thin-film of LN bonded to SiO_2 on a Si substrate.

Alternatively, micro-platelets may be exfoliated in the absence of a handle wafer. The micro-platelets can then be transferred in a pick-and-place scheme to specific locations on pre-patterned dies [58], [59]. Naturally, the former wafer-bonding approach is more scalable than the latter technique. Wafers of thin-film LN on Si substrates [54] are of more technological interest than thin-film LN on LN substrates [55]. The latter technology on LN substrates is sometimes called LN on insulator (LNOI). Nowadays, 75-mm diameter thin-film LN wafers are commercially available on both LN and Si substrates. 150-mm diameter thin-film LN wafers may be available soon – the bonding process is repeatable and reliable, and 150-mm single crystalline LN wafers are already available.

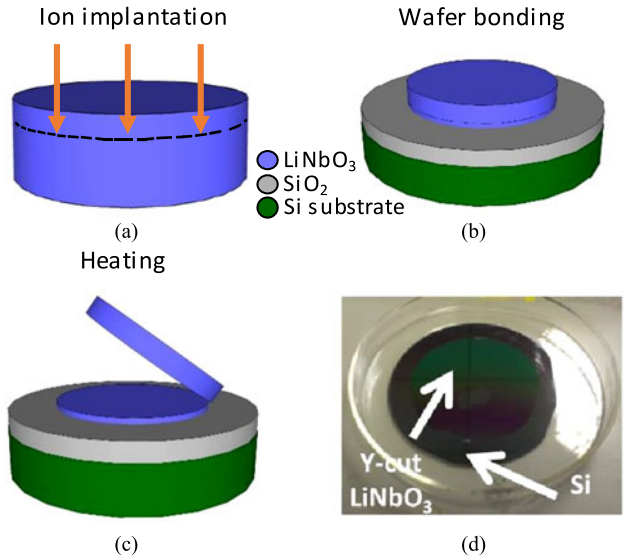

Fig. 4. Fabrication of thin-film LN on Si wafers. (a) Helium ion implantation on a single crystal LN wafer. (b) The implanted LN wafer is bonded to an oxidized Si wafer. (c) Heated to thermally exfoliate a thin-film of LN around the implantation peak. (d) A fully-processed 3-inch X-cut LN thin-film bonded to an oxidized 4-inch Si wafer. [54], [57].

IV. Heterogeneous Integration of Thin-Film Lithium Niobate

Heterogeneous integration has enabled significant advances in integrated photonics [60]–[63]. In the context of thin-film LN, heterogeneous integration has been used to form rib-loaded waveguides for electrooptics [54], [63]–[67], $\chi^{(2)}$-based nonlinear optics [57], [68]–[70], and third-order or $\chi^{(3)}$-based nonlinear optics [71], [72]. Rib-loading thin-film LN with an easy-to-process material is one of the most straightforward routes to forming thin-film LN waveguides. It circumvents the need to process the LN directly, and avoids the limited optical confinement of the aforementioned diffused waveguides [73]. While recent efforts have realized low loss thin-film LN waveguides

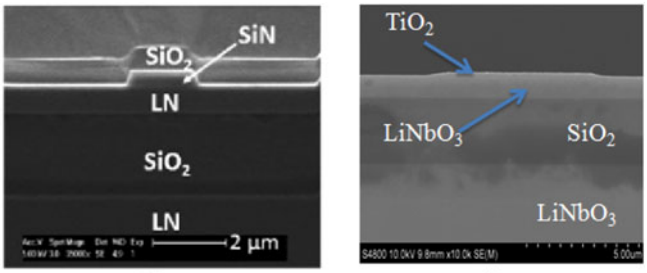

Fig. 5. Scanning-electron micrographs of directly deposited thin-film LN waveguides using (a) silicon nitride [69], and (b) titanium dioxide [88].

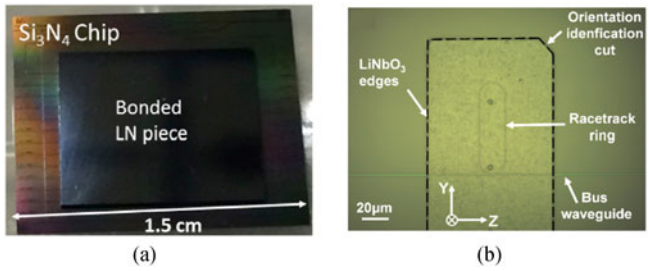

Fig. 6. (a) Micrograph of a ~1 cm^2 LN thin film bonded onto a LPCVD SiN chip [71]. (b) Scanning electron micrograph of a micron-scale thin-film LN platelet bonded onto a SOI racetrack resonator [91].

by etching LN [74], [75], the rib-loading approach is simpler and is far more commonly used. Results from both rib-loaded and etched-LN are included in Section V for completeness. Direct thin-film deposition and bonding are the two main methods that are used for heterogeneous LN integration, encompassing a very wide range of materials, as follows

A. Direct Thin-Film Deposition

Direct deposition has been used to integrate thin-film LN with a variety of materials, such as plasma-enhanced chemical vapor deposited (PECVD) silicon nitride (SiN), amorphous silicon (a-Si), chalcogenide glass (ChG), tantalum pentoxide (Ta_2O_5), and titanium dioxide (TiO_2), using a range of deposition techniques, as follows.

PECVD is a mature technique that has been used for making integrated photonic devices at a range of temperatures from room temperature to over 300 °C, offering a photonic-foundry compatible process. PECVD SiN has been used as a passive rib-loading dielectric for electrooptic modulation [66], [67] and nonlinear frequency conversion [57], [68]–[70] in thin-film LN (Fig. 5(a)). Interestingly, PECVD SiN can be used for more than passive rib-loading [76], [77]. It is a versatile material whose stoichiometry can be altered through deposition conditions [78], [79], thereby tuning the refractive index, dispersion, optical bandgap, and the $\chi^{(3)}$ susceptibility. For example, the nonlinear refractive index, n_2, which directly scales with $\chi^{(3)}$, can be up to ~500 times higher in silicon-rich SiN compared to stoichiometric SiN [79]. Amorphous silicon, which can be considered the extreme case of silicon-rich PECVD SiN, has been deposited via PECVD on thin-film LN [80].

Chalcogenide glasses, such as $Ge_{23}Sb_7S_{70}$, a germanium-antimony-sulfide glass [80]–[84], have been used for passive rib-loading on thin-film LN to form electrooptic MZ and microring modulators [64], [65]. ChG itself has been used for supercontinuum generation [83] and flexible photonics [84]. ChG on thin-film LN is also being explored for demonstrations of $\chi^{(3)}$ nonlinear optics, such as four-wave mixing and supercontinuum generation, which benefit from the high $\chi^{(3)}$ coefficient of ChG [85]. ChG can be reliably deposited by both electron-beam and thermal evaporation at low temperatures (< 400 °C).

Ta_2O_5 and TiO_2 have been used for rib-loading thin-film LN as well [54], [86]–[88] (Fig. 5(b)). Both materials have strong potential for $\chi^{(3)}$ nonlinear optics on thin-film LN, and can be deposited by sputtering or evaporation and post-deposition oxidation of the constituent metals. Alternatively, reactive sputtering may be used.

B. Thin-Film Bonding

The deposition conditions of certain materials are incompatible with thin-film LN. An example is low-pressure chemical vapor deposited (LPCVD) SiN. LPCVD SiN, a popular alternative to PECVD SiN, has been used for numerous demonstrations of ultra-low loss waveguides, and $\chi^{(3)}$ nonlinear optics such as four-wave mixing, supercontinuum generation, and frequency comb generation, among others [89], [90]. The stoichiometry of LPCVD SiN can be varied, similar to PECVD SiN. LPCVD SiN is usually deposited around 800 °C, a temperature that, due to differences in thermal expansion, would crack LN thin films on Si.

Chip- and wafer-scale bonding is the most straightforward way to integrate materials with thin-film LN that cannot be directly deposited (Fig. 6). For example, thin-film LN on Si chips have been bonded, mediated by SiO_2, to LPCVD SiN chips [71], followed by removal of the Si substrate and SiO_2 cladding. Similarly, chip and platelet scale bonding is the method of choice for integrating thin-film LN with silicon photonics. Microplatelets of free-standing thin-film LN have been bonded onto silicon microrings to form EO modulators [59], [91]. Chips of thin-film LN have been bonded, but without substrate removal, to waveguides on the silicon-on-insulator (SOI) platform [92].

The reduction in bending radius offered by heterogeneous integration of thin-film LN compared to conventional LN waveguides is shown in Fig. 7.

V. Thin-Film LN Optical Modulators and Nonlinear Frequency Converters

A. Electrooptic Modulators

EO modulators using thin-film LN have been a subject of intense investigation in the past years, and the overall performance of thin-film EO modulators is on par with commercial off-the-shelf (COTS) EO modulators [63]. A number of parameters qualify the performance of EO modulators, shown in Fig. 8. These include the drive voltage/power consumption, or half-wave voltage via the half-wave voltage length product, $V_\pi L$, (Fig. 8(a) and 8(c)) tunability for resonant

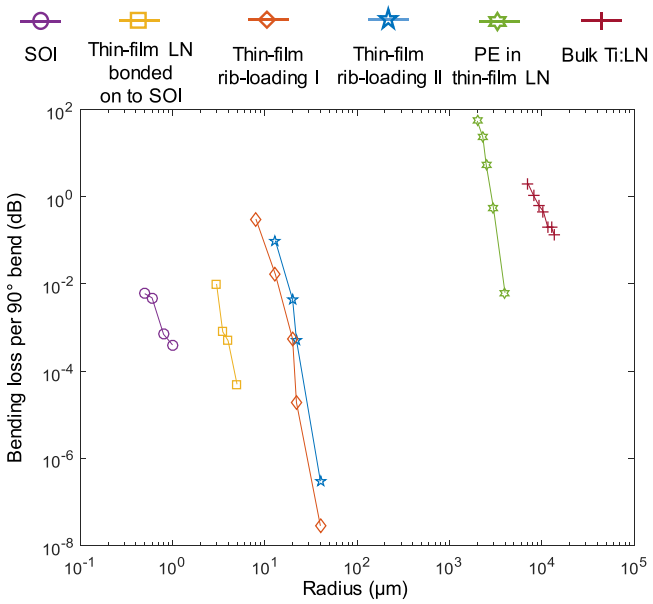

Fig. 7. Bending loss variation with bending radius for different heterogeneously integrated thin-film LN platforms. Based on the high refractive index of silicon, the thin-film LN bonded on to SOI can offer the lowest bending radii by trading off the fraction of the optical power confined in the LN thin-film with the bending radius (data extracted from [92]). The rib-loaded structures offer bending radii around 20 μm (data extracted from [63]). Proton-exchanged waveguides in both thin-film and bulk LN have bending radii > 2000 μm (data extracted from [73] and [93]). Clearly, thin-film LN offers orders of magnitude improvement in bending losses. Details of the exact structures used can be found in the respective references.

structures, 3-dB modulation bandwidth (Fig. 8(b) and 8(d)), optical insertion loss, optical extinction ratio, optical bandwidth, chirp, and optical bandwidth. Specific applications have additional performance metrics. For example, the electrical extinction ratio (EER) is central to long-reach digital transmission, while link linearity and modulator linearity are key in RF photonic links. Short-reach datacom links have significantly relaxed EER requirements compared to long-reach transmission. The device footprint is important for the integration of multiple modulators to form complex photonic integrated circuits (PIC).

There are two major types of modulators – travelling wave, for example MZ modulators, and resonant, such as microring modulators. Depending on the application and the desired level of on-chip integration, either MZ, or microring modulators may be preferable. In some cases, combinations of both may be advantageous. MZ modulators usually have higher extinction ratios and modulation bandwidths relative to microring modulators. However, apart from the reduced device footprint, microring modulators require simple RF electrode design, centered primarily on the resistive-capacitive (RC) time constant. Travelling wave electrode design is more involved, with impedance matching, RF metal loss, and velocity matching between the optical and RF mode being important factors. Fortunately, thin-film LN offers near intrinsic velocity matching, circumventing the need for buffer layers as used in COTS LN MZ modulators. In addition, the refractive index of the rib material can be adjusted as required to fine-tune the velocity matching.

A comprehensive review of thin-film LN EO modulators along with a detailed analysis of performance metrics and guidelines for design can be found in [63]. Here, we briefly summarize the state-of-the-art in Table III, which details the aforementioned performance metrics of two of the best performing thin-film MZ and microring modulators, and of COTS MZ modulators. Evidently, the performance of thin-film LN EO modulators is better than or comparable to the COTS counterparts.

B. Nonlinear Frequency Converters

Second-order nonlinear optics on silicon is still a nascent field. There have been only a handful of demonstrations of $\chi^{(2)}$ -based frequency conversion on silicon substrates, a few of which have employed thin-film LN. A detailed review of SHG on silicon substrates along with detailed descriptions of phase-matching and comparisons of LN to other nonlinear optical materials can be found in [57]. Briefly, only a few compound semiconductors, like GaAs, have nonlinear coefficients larger LN's. However, addressing the phase matching issue has been challenging for compound semiconductors. Hence, LN has been the dominant material for second-order nonlinear optics. Here, we focus on SHG in thin-film LN on both Si and LN substrates. A variety of PM techniques have been employed for implementing SHG, including quasi-phase matching (QPM) by periodic poling (Fig. 9(a)–9(d)), mode-shape modulation (Fig. 9(e)–9(g)), grating-assisted QPM (Fig. 9(h)), modal dispersion engineering (Fig. 9(i)–9(l)), cyclic PM and modal dispersion in microresonators (Fig. 10(a)–10(c)), and grating induced mode conversion (Fig. 10(d) and 10(e)). SHG is arguably the easiest of the $\chi^{(2)}$ phenomena to experimentally verify, and is therefore broadly employed for first and proof-of-concept demonstrations.

Of the various methods listed in Table IV, periodic poling (in conventional LN crystals) has arguably been used most widely for nonlinear frequency conversion in both research and commercial settings. Periodic poling relies on a regular periodic reversal of the ferroelectric domain, where the sign of the relevant coefficient of the $\chi^{(2)}$ tensor alternates in sign, and has been successfully adapted to thin-film LN [68], [69].

However, poling relies on ferroelectricity and not all $\chi^{(2)}$ nonlinear materials are ferroelectric, i.e., there are materials like gallium arsenide that cannot be poled. An alternative method for QPM in such materials is mode-shape modulation [70] and grating-assisted QPM [98]. This approach relies on perturbation of the nonlinear medium, or the interacting waveguide modes, to induce a periodic variation in the nonlinear overlap integral for QPM [57]. Perfect PM can be achieved by engineering the mode dispersion of the nonlinear waveguide to realize zero phase mismatch between the interacting optical modes. However, this comes at the cost of using a higher-order mode at the lower wavelength(s) to compensate for material dispersion, thereby compromising the nonlinear overlap and the nonlinear efficiency [99], [100].

Microresonators have been used in attempts to enhance the nonlinear interaction, where PM has been effected via cyclic PM [100] and modal dispersion [102]. However, the demonstrations

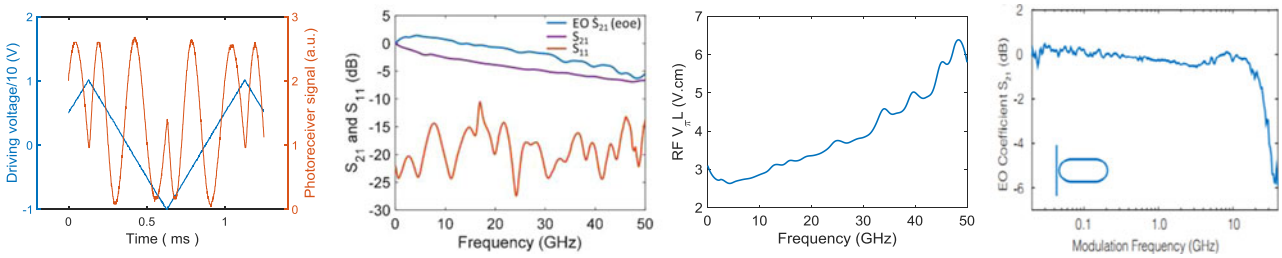

Fig. 8. Thin-film LN Mach-Zehnder modulator. (a) Half-wave voltage length product ($V\pi$ L) of 3.1 V.cm. (b) S-parameters showing 33 GHz 3-dB modulation bandwidth. (c) RF half-wave voltage length product up to 50 GHz [66]. (d) EO S-parameter of a thin-film LN microring racetrack modulator [94].

TABLE III
COMPARISON OF THIN-FILM LN AND CONVENTIONAL LN EO MODULATORS

Property	Thin-film Mach-Zehnder [66]	Thin-film Microring [94]	COTS Mach-Zehnder
3-dB modulation bandwidth (GHz)	33	30	25 – 70 [52,95,96]
DC half-wave voltage length product (V.cm)	3.1	NA	~10 [52,95,96]
RF half-wave voltage length product (V.cm)	< 6.5 (at 50 GHz)	NA	NA
Tunability (pm/V)	NA	7	NA
Optical extinction ratio (dB)	18	3	> 20 [52,96,97]
Linearity in 1 to 10 GHz (dB.$Hz^{2/3}$)	~95	NA	90 – 120 [98]
NRZ transmission (Gbps)	NA	40 (3-dB extinction)	40 [52,95]
Waveguide loss (dB/cm)	1	3	0.2 – 0.5 [44,45]

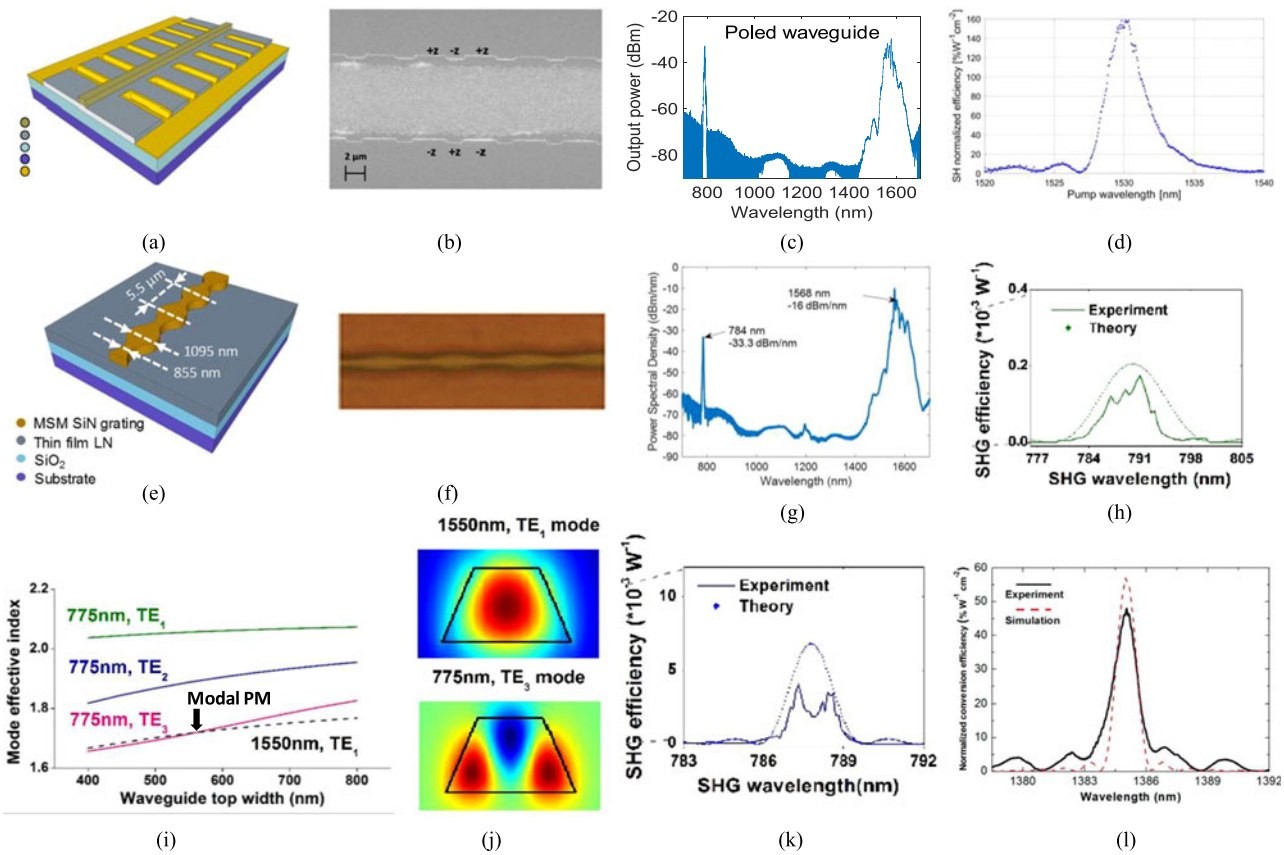

Fig. 9. Periodically-poled thin-film LN [68], [69]: (a) schematic [68]; (b) scanning-electron micrograph showing ferroelectric domain reversal [68]; (c) optical spectrum showing SHG [68]; and (d) SHG tuning curve [69]. Mode shape modulation: (e) schematic [70]; (f) micrograph showing grating waveguide [70]; and (g) optical spectrum showing SHG [70]. (h) SHG tuning curve of grating assisted QPM [99]. Modal dispersion engineering: (i) simulation showing point of modal PM of the modes shown in (j), and, (k) [99] and (l) [100] are two modal PM based SHG tuning curves.

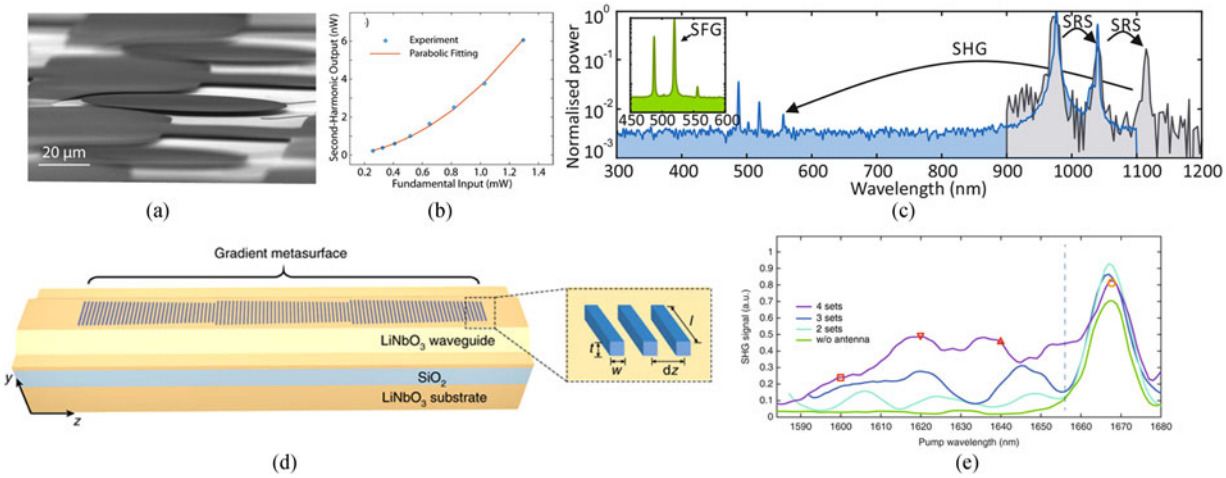

Fig. 10. Cyclic PM and modal dispersion in microresonators [101], [102]: (a) scanning-electron micrograph [101], and SHG outputs ((b) [101] and (c) [102]). Grating-induced mode conversion: (d) schematic [103], and (e) SHG output [103].

TABLE IV
COMPARISON OF DIFFERENT APPROACHES TO NONLINEAR OPTICAL FREQUENCY CONVERSION IN THIN-FILM LN

Phase-matching Technique	Substrate	Efficiency	Comments
Periodic poling [68,69]	Si & LN	Up to 160% $W^{-1}cm^{-2}$	Maximum nonlinear mode overlap can be utilized.
Mode-shape modulation [70] & Grating-assisted QPM [99]	Si & LN	Up to 12% $W^{-1}cm^{-2}$	Nonlinear efficiency must be balanced with grating-induced propagation loss.
Modal dispersion engineering [99,100]	LN	Up to 48% $W^{-1}cm^{-2}$	Typically uses higher-order modes for PM, which reduces the nonlinear mode overlap.
Modal and cyclic PM in microresonators [101,102]	LN	Up to 0.36% W^{-1}	Limited to high free-spectral range and high-quality factor resonant cavities, and the conversion bandwidth is limited by the cavity linewidth.
Grating-induced mode conversion [103]	LN	Up to 1600% $W^{-1}cm^{-2}$	Limited to ~ 50 μm length, leading to overall low device efficiency. Also limited by high losses of ~ 900 dB/cm at the second harmonic wavelength.

reported so far have yet to realize the full efficiency enhancement offered by resonant confinement.

Finally, grating-induced mode conversion has been utilized for SHG, but this approach at present is accompanied by prohibitive propagation losses of 10% per 5 μm, corresponding to ~900 dB/cm [103].

Each of the above methods requires precise fabrication to achieve high conversion efficiency at the desired wavelengths, and comes with its own merits and shortcomings. A study on the effects of fabrication tolerances on the efficiency of QPM, applied to conventional PPLN devices, can be found in [104]. The nonlinear conversion efficiency (see [57] for a formal definition and analysis) is the main metric that is used to compare the performance of nonlinear frequency converters. However, there are other considerations such as the nonlinear conversion bandwidth. It is interesting to note that the conversion bandwidth decreases with increasing pump depletion [105]. Overall, the conversion bandwidth is constrained by PM, pump depletion or conversion efficiency, and the use of resonant configurations.

VI. OUTLOOK

Thin-film LN integrated photonics has enabled several noteworthy advancements in the miniaturization and efficiency enhancement of EO modulators and nonlinear frequency converters. Along with these achievements, heterogeneous thin-film LN integration has also facilitated the incorporation of high $\chi^{(3)}$ materials for advanced nonlinear applications [71], [72]. In keeping with the integration schemes discussed in Section IV, the integration of quantum dots [106], typical III-V epitaxial structures, and other desirable functional materials with thin-film LN is an attractive proposition.

Small-footprint LN EO modulators now operate with low drive voltages of around 1 V, high extinction ratios of over 20 dB, high modulation bandwidths of up to 33 GHz, and modulation up to 110 GHz. However, optical and electrical packaging, thermal and DC drift [107]–[109], and overall reliability are some key concerns that need to be studied and potentially addressed for commercial viability. Some of the potential applications are: (a) telecommunications, as optical interconnects in data centers, as low power switches, and terrestrial and sub-marine links [7]–[9], [110]; (b) highly-linear RF-photonic links integrated into vehicles [111], [112]; (c) millimeter-wave beam formation and imaging [113]; and (d) high sensitivity electric field sensors [114].

Simultaneously, a variety of efficient nonlinear optical frequency converters have been realized, as discussed in the previous section. The emergent pursuit of second-order nonlinear submicron integrated photonics holds tremendous promise in diverse applications, including: (a) efficient coherent links

between near-infrared and visible frequencies for optical self-referencing frequency metrology [115], [116]; (b) mid-infrared light generation for spectroscopy [117]; (c) quantum photonics at telecom wavelengths [118], [119]; (d) high-harmonic generation [120], which establishes a link between mid-infrared and ultraviolet frequencies; (e) engineering optical frequency conversion in semiconductor and polycrystalline materials [70], [121]; and (f) efficient optical parametric oscillators [122].

Apart from EO and nonlinear optical applications, thin-film LN may lead to further novel investigations of the material properties of LN [123]–[125] and demonstrations of sensors [126].

In addition to stand-alone applications of LN photonic devices, a wide variety of integrated optical systems may be envisioned, encouraged by the demonstrated potential of silicon photonic integration. Increased data rates can be addressed by higher order modulation formats that require composite modulators comprised of combinations of phase and amplitude modulators. Ultracompact LN modulators are very attractive for such applications because of their small device footprint and low power consumption. Compatibility with silicon photonic foundry processes may require solutions that introduce LN in the BEOL stage of fabrication.

In a similar vein, cascaded nonlinear devices on the same LN chip can generate entangled photon states beyond two-photon states. Moreover, the possibility of realizing EO and nonlinear optical functions in a single LN PIC heralds the realization of sources of complex entangled quantum optic states of light that can be dynamically tuned via the EO effect. EO circuits could be also utilized for further on-chip processing and manipulation.

VII. Conclusion

Thin film technologies have rejuvenated lithium niobate photonics in the past years and have made the versatile material a competing candidate for modern integrated platforms. Improvements in electrical and optical efficiency have been realized in electrooptics and nonlinear optics, respectively, as a direct consequence of the increased optical confinement. The compact electrooptic modulators perform as well as commercial-off-the-shelf counterparts, with smaller footprints, lower switching voltages, and comparable digital and analog operation. Also, efficient nonlinear optical frequency converters have been developed based on the high-contrast thin-film waveguide. These devices can be integrated on silicon, with small bending radii, and are ideal for forming densely heterogeneous photonic integrated circuits.

Acknowledgment

The authors would like to thank the DARPA DODOS Program, the ONR Young Investigator Program, Harris Corporation and the NSF, DOE, and NASA SBIR Programs. The views, opinions, and/or findings expressed are those of the authors and should not be interpreted as representing the official views or policies of the Department of Defense or the U.S. Government.

References

[1] E. L. Wooten *et al.*, "A review of lithium niobate modulators for fiber-optic communications systems," *IEEE J. Sel. Topics Quantum Electron.*, vol. 6, no. 1, pp. 69–82, Jan. 2000.

[2] M. M. Fejer, "Nonlinear optical frequency conversion," *Phys. Today*, vol. 47, no. 5, pp. 25–32, May 1994.

[3] R. W. Boyd, *Nonlinear Optics*. New York, NY, USA: Academic Press, 2003.

[4] M. Izutsu, Y. Yamane, and T. Sueta, "Broad-band traveling-wave modulator using a $LiNbO_3$ optical waveguide," *IEEE J. Quantum Electron.*, vol. QE-13, no. 4, pp. 287–290, Apr. 1977.

[5] F. J. Leonberger, "High-speed operation of $LiNbO_3$ electrooptic interferometric waveguide modulators," *Opt. Lett.*, vol. 5, no. 7, pp. 312–314, Jul. 1980.

[6] R. E. Tench *et al.*, "Performance evaluation of waveguide phase modulators for coherent systems at 1.3 and 1.5 microns," *J. Lightw. Technol.*, vol. LT-5, no. 4, pp. 492–501, Apr. 1987.

[7] D. J. Blumenthal, P. R. Prucnal, L. Thylen, and P. Granestrand, "Performance of and 8×8 $LiNbO_3$ switch matrix as a gigahertz self-routing switching node," *Electron. Lett.*, vol. 23, no. 25, pp. 1359–1360, Dec. 1987.

[8] I. Sawaki *et al.*, "Rectangularly configured 4×4 Ti: $LiNbO_3$ matrix switch with low drive voltage," *IEEE J. Sel. Commun.*, vol. 6, no. 7, pp. 1267–1272, Aug. 1988.

[9] H. Nishimoto, M. Iwasaki, S. Suzuki, and M. Konodo, "Polarization independent $LiNbO_3$ 8×8 matrix switch," *IEEE Photon. Technol. Lett.*, vol. 2, no. 9, pp. 634–636, Sep. 1990.

[10] L. E. Myers *et al.*, "Quasi-phase-matched 1.064-μm-pumped optical parametric oscillator in bulk periodically poled $LiNbO_3$," *Opt. Lett.*, vol. 20, no. 1, pp. 52–54, Jan. 1995.

[11] L. E. Myers, R. C. Eckardt, M. M. Fejer, R. L. Byer, and W. R. Bosenberg, "Multigrating quasi-phase-matched optical parametric oscillator in periodically poled $LiNbO_3$," *Opt. Lett.*, vol. 21, no. 8, pp. 591–593, Apr. 1996.

[12] G. D. Miller *et al.*, "42%-efficient single-pass cw second-harmonic generation in periodically poled lithium niobate," *Opt. Lett.*, vol. 22, no. 24, pp. 1834–1836, Dec. 1997.

[13] J. Webjörn, F. Laurell, and G. Arvidsson, "Fabrication of periodically domain-inverted channel waveguides in lithium niobate for second harmonic generation," *IEEE J. Lightw. Technol.* vol. 7, no. 10, pp. 1597–1600, Oct. 1989.

[14] E. J. Lim, M. M. Fejer, R. L. Byer, and W. J. Kozlovsky, "Blue light generation by frequency doubling in periodically poled lithium niobate channel waveguide," *Electron. Lett.* vol. 25, no. 11, pp. 731–732, May 1989.

[15] E. J. Lim, M. M. Fejer, and R. L. Byer, "Second-harmonic generation of green light in periodically poled planar lithium niobate waveguide," *Electron. Lett.*, vol. 25, no. 3, pp. 174–175, Feb. 1989.

[16] Y. H. Chen and Y. C. Huang, "Actively Q-switched Nd:YVO_4 laser using an electro-optic periodically poled lithium niobate crystal as a laser Q-switch," *Opt. Lett.*, vol. 28, no. 16, pp. 1460–1462, Aug. 2003.

[17] Y. Y. Lin *et al.*, "Electro-optic periodically poled lithium niobate Bragg modulator as a laser Q-switch," *Opt. Lett.*, vol. 32, no. 5, pp. 545–547, Mar. 2007.

[18] S. T. Lin *et al.*, "Monolithically integrated laser Bragg Q-switch and wavelength converter in a PPLN crystal," *Opt. Express*, vol. 15, no. 25, pp. 17093–17098, Dec. 2007.

[19] S. Tanzilli *et al.*, "Highly efficient photon-pair source using periodically poled lithium niobate waveguide," *Electron. Lett.*, vol. 37, no. 1, pp. 26–28, Jan. 2001.

[20] S. Tanzilli *et al.*, "PPLN waveguide for quantum communication," *Eur. Phys. J. D*, vol. 18, no. 2, pp. 155–160, Feb. 2002.

[21] J. Czochralski, "Ein neues Verfahren zur Messung der Kristallisationsgeschwindigkeit der Metalle," *Z. Phys. Chem.*, vol. 92, no. 1, pp. 219–221, Nov. 1918.

[22] A. A. Ballman, "Growth of piezoelectric and ferroelectric materials by Czochralski technique," *J. Amer. Ceram. Soc.*, vol. 48, no. 2, pp. 112–113, Feb. 1965.

[23] K. Nassau, H. J. Levinstein, and G. M. Loiacono, "Ferroelectric lithium niobate. 1. Growth, domain structure, dislocations and etching," *J. Phys. Chem. Solids*, vol. 27, no. 6–7, pp. 983–988, Jun./Jul. 1966.

[24] K. Nassau, H. J. Levinstein, and G. M. Loiacono, "Ferroelectric lithium niobate. 2. Preparation of single domain crystals," *J. Phys. Chem. Solids*, vol. 27, no. 6/7, pp. 989–996, Jun./Jul. 1966.

[25] S. C. Abrahams, J. M. Reddy, and J. L. Bernstein, "Ferroelectric lithium niobate. 3. Single crystal X-ray diffraction study at 24 °C," *J. Phys. Chem. Solids*, vol. 27, no. 6–7, pp. 997–1012, Jun./Jul. 1966.

[26] S. C. Abrahams, W. C. Hamilton, and J. M. Reddy, "Ferroelectric lithium niobate. 4. Single crystal neutron diffraction study at 24 °C," *J. Phys. Chem. Solids*, vol. 27, no. 6/7, pp. 1013–1018, Jun./Jul. 1966.

[27] S. C. Abrahams, H. J. Levinstein, and J. M. Reddy, "Ferroelectric lithium niobate. 5. Polycrystal X-ray diffraction study between 24° and 1200 °C," *J. Phys. Chem. Solids*, vol. 27, no. 6/7, pp. 1019–1026, Jun./Jul. 1966.

[28] P. V. Lenzo, E. G. Spencer, and K. Nassau, "Electrooptic coefficients in single-domain ferroelectric lithium niobate," *J. Opt. Soc. Amer.*, vol. 56, no. 5, pp. 633–635, May 1966.

[29] G. D. Boyd, R. C. Miller, K. Nassau, W. L. Bond, and A. Savage, "$LiNbO_3$: An efficient phase matchable nonlinear optical material," *Appl. Phys. Lett.*, vol. 5, no. 11, pp. 234–236, Dec. 1964.

[30] L. O. Svaasand, M. Eriksrud, G. Nakken, and A. P. Grande, "Solid-solution range of $LiNbO_3$," *J. Crystal Growth*, vol. 22, no. 3, pp. 230–232, May 1974.

[31] R. S. Weis and T. K. Gaylord, "Lithium niobate: Summary of physical properties and crystal structure," *Appl. Phys. A*, vol. 37, no. 4, pp. 191–203, Aug. 1985.

[32] D. A. Bryan, R. Gerson, and H. E. Tomaschke, "Increased optical damage resistance in lithium niobate," *Appl. Phys. Lett.*, vol. 44, pp. 847–849, 1984.

[33] Y. Kong, J. Wen, and H. Wang, "New doped lithium niobate crystal with high resistance to photorefraction—$LiNbO_3$:In," *Appl. Phys. Lett.*, vol. 66, no. 3, pp. 280–281, Jan. 1995.

[34] T. R. Volk, V. I. Pryalkin, and N. M. Rubinina, "Optical-damage-resistant $LiNbO_3$:Zn crystal," *Opt. Lett.*, vol. 15, no. 18, pp. 996–998, Sep. 1990.

[35] T. Volk, N. Rubinina, and M. Wöhlecke, "Optical-damage-resistant impurities in lithium niobate," *J. Opt. Soc. Amer. B*, vol. 11, no. 9, pp. 1681–1687, Sep. 1994.

[36] Y. Konga *et al.*, "Highly optical damage resistant crystal: Zirconium-oxide-doped lithium niobate," *Appl. Phys. Lett.*, vol. 91, no. 8, Aug. 2007, Art. no. 081908.

[37] S. Li *et al.*, "The optical damage resistance and absorption spectra of LiNbO3:Hf crystals," *J. Phys. Condens. Matter*, vol. 18, no. 13, pp. 3527–3534, Apr. 2006.

[38] L. Wang *et al.*, "Increased optical-damage resistance in tin-doped lithium niobate," *Opt. Lett.*, vol. 35, no. 6, pp. 883–885, Mar. 2010.

[39] M. Born and E. Wolf, *Principles of Optics*, 6th ed. Oxford: Pergamon Press, 1980.

[40] D. E. Zelmon, D. L. Small, and D. Jundt, "Infrared corrected Sellmeier coefficients for congruently grown lithium niobate and 5 mol. % magnesium oxide–doped lithium niobate," *J. Opt. Soc. Amer. B*, vol. 14, no. 12, pp. 3319–3322, Dec. 1997.

[41] F. Pockels, *Lehrbuch der Kristalloptik*. Leipzig und Berlin: B. G. Teubner, 1906

[42] W. S. Chang, *Fundamentals of Guided-Wave Optoelectronic Devices*. Cambridge, U.K.: Cambridge Univ. Press, 2010.

[43] M. Fukuma, J. Noda, and H. Iwasaki, "Optical properties in titanium-diffused $LiNbO_3$ strip waveguides," *J. Appl. Phys.*, vol. 49, no. 7, pp. 3693–3698, Jul. 1978.

[44] T. Nozawa, K. Noguchi, H. Miyazawa, and K. Kawano, "Water vapor effects on optical characteristics in Ti:$LiNbO_3$ channel waveguides," *Appl. Opt.*, vol. 30, no. 9, pp. 1085–1089, Mar. 1991.

[45] M. Fukuma and J. Noda, "Optical properties of titanium-diffused $LiNbO_3$ strip waveguides and their coupling-to-a-fiber characteristics," *Appl. Opt.*, vol. 19, no. 4, pp. 591–597, Feb. 1980.

[46] R. C. Alferness, L. L. Buhl, and M. D. Divino, "Low-loss fiber-coupled waveguide directional coupler modulator," *Electron. Lett.*, vol. 18, no. 12, pp. 490–491, Jun. 1982.

[47] V. Ramaswamy, R. C. Alferness, and M. Divino, "High efficiency single-mode fibre to Ti:$LiNbO_3$ waveguide coupling," *Electron. Lett.*, vol. 18, no. 1, pp. 30–31, Jan. 1982.

[48] J. L. Jackel, C. E. Rice, and J. J. Veselka, "Proton exchange for high-index waveguides in $LiNbO_3$," *Appl. Phys. Lett.*, vol. 41, no. 7, pp. 607–608, Oct. 1982.

[49] P. G. Suchoski, T. K. Findakly, and F. J. Leonberger, "Stable low-loss proton-exchanged $LiNbO_3$ waveguide devices with no electro-optic degradation," *Opt. Lett.*, vol. 13, no. 11, pp. 1050–1052, Nov. 1988.

[50] M. L. Bortz and M. M. Fejer, "Annealed proton-exchanged $LiNbO_3$ waveguides," *Opt. Lett.*, vol. 16, no. 23, pp. 1844–1846, Dec. 1991.

[51] Y. N. Korkishko *et al.*, "Reverse proton exchange for buried waveguides in LiNbO3," *J. Opt. Soc. Amer. A.*, vol. 15, no. 7, pp. 1838–1842, Jul. 1998.

[52] K. Noguchi, O. Mitomi, and H. Miyazawa, "Millimeter-wave Ti:$LiNbO_3$ optical modulators," *J. Lightw. Technol.*, vol. 16, no. 4, pp. 615–619, Apr. 1998.

[53] M. Levy *et al.*, "Fabrication of single-crystal lithium niobate films by crystal ion slicing," *Appl. Phys. Lett.*, vol. 73, no. 16, pp. 2293–2295, Oct. 1998.

[54] P. Rabiei, J. Ma, S. Khan, J. Chiles, and S. Fathpour, "Heterogeneous lithium niobate photonics on silicon substrates," *Opt. Express*, vol. 21, no. 21, pp. 25573–25581, Oct. 2013.

[55] P. Rabiei and P. Günter, "Optical and electro-optical properties of submicrometer lithium niobate slab waveguides prepared by crystal ion slicing and wafer bonding," *Appl. Phys. Lett.*, vol. 85, no. 20, pp. 4603–4605, Nov. 2004.

[56] H. Hu, L. Gui, R. Ricken, and W. Sohler, "Towards nonlinear photonic wires in lithium niobate," *Proc. SPIE*, vol. 7604, 2010, Art. no. 76040R, doi: 10.1117/12.842674.

[57] A. Rao, and S. Fathpour, "Second-harmonic generation in integrated photonics on silicon," *Phys. Status Solidi A*, vol. 215, Art. no. 1700684, 2017.

[58] Y. S. Lee *et al.*, "Hybrid Si-$LiNbO_3$ microring electro-optically tunable resonators for active photonic devices," *Opt. Lett.*, vol. 36, no. 7, pp. 1119–1121, Apr. 2011.

[59] L. Chen, M. G. Wood, and R. M. Reano, "12.5 pm/V hybrid silicon and lithium niobate optical microring resonator with integrated electrodes," *Opt. Express*, vol. 21, no. 22, pp. 27003–27010, Nov. 2013.

[60] D. Liang and J. E. Bowers, "Recent progress in lasers on silicon," *Nature Photon.*, vol. 4, pp. 511–517, Jul. 2010.

[61] M. J. R. Heck *et al.*, "Hybrid silicon photonic integrated circuit technology," *IEEE J. Sel. Topics Quantum Electron.*, vol. 19, no. 4, Jul./Aug. 2013, Art. no. 6100117.

[62] S. Fathpour, "Emerging heterogeneous integrated photonic platforms on silicon," *Nanophotonics*, vol. 4, no. 1, pp. 143–164, May 2015.

[63] A. Rao and S. Fathpour, "Compact lithium niobate electrooptic modulators," *IEEE J. Sel. Topics Quantum Electron.*, vol. 24, no. 4, Jul./Aug. 2018, Art. no. 3400114.

[64] A. Rao *et al.*, "Heterogeneous microring and Mach-Zehnder lithium niobate electro-optical modulators on silicon," in *Proc. Conf. Lasers Electro-Opt.*, 2015, Paper STu2F.4.

[65] A. Rao *et al.*, "Heterogeneous microring and Mach-Zehnder modulators based on lithium niobate and chalcogenide glasses on silicon," *Opt. Express*, vol. 23, no. 17, pp. 22746–22752, Aug. 2015.

[66] A. Rao *et al.*, "High-performance and linear thin-film lithium niobate Mach–Zehnder modulators on silicon up to 50 GHz," *Opt. Lett.*, vol. 41, no. 24, pp. 5700–5703, Dec. 2016.

[67] S. Jin, L. Xu, H. Zhang, and Y. Li, "$LiNbO_3$ thin-film modulators using silicon nitride surface ridge waveguides," *IEEE Photon. Technol. Lett.*, vol. 28, no. 7, pp. 736–739, Apr. 2016.

[68] A. Rao *et al.*, "Second-harmonic generation in periodically-poled thin film lithium niobate wafer-bonded on silicon," *Opt. Express*, vol. 24, no. 26, pp. 29941–29947, Dec. 2016.

[69] L. Chang *et al.*, "Thin film wavelength converters for photonic integrated circuits," *Optica*, vol. 3, no. 5, pp. 531–535, May 2016.

[70] A. Rao *et al.*, "Second-harmonic generation in single-mode integrated waveguides based on mode-shape modulation," *Appl. Phys. Lett.*, vol. 110, no. 11, Mar. 2017, Art. no. 111109.

[71] L. Chang *et al.*, "Heterogeneous integration of lithium niobate and silicon nitride waveguides for wafer-scale photonic integrated circuits on silicon," *Opt. Lett.*, vol. 42, no. 4, pp. 803–806, Feb. 2017.

[72] A. Honardoost *et al.*, "Heterogeneous integration of thin-film lithium niobate and chalcogenide waveguides on silicon," in *Proc. IEEE Photon. Conf.*, 2017, pp. 545–546.

[73] R. F. Tavlykaev, K. Kueckelhaus, and E. I. Voges, "Index profile reconstruction of Ti:$LiNbO_3$ structures and bending loss evaluation from near-field measurements," *Proc. SPIE*, vol. 2150, May 1994, pp. 263–270.

[74] M. Zhang, C. Wang, R. Cheng, A. Shams-Ansari, and M. Lončar, "Monolithic ultra-high-Q lithium niobate microring resonator," *Optica*, vol. 4, no. 12, pp. 1536–1537, Dec. 2017.

[75] I. Krasnokutska, J.-L. J. Tambasco, X. Li, and A. Peruzzo, "Ultra-low loss photonic circuits in lithium niobate on insulator," *Opt. Express*, vol. 26, no. 2, pp. 897–904, Jan. 2018.

[76] Y. Huang, J. Song, X. Luo, T.-Y. Liow, and G.-Q. Lo, "CMOS compatible monolithic multi-layer Si_3N_4 -on-SOI platform for low-loss high performance silicon photonics dense integration," *Opt. Express*, vol. 22, no. 18, pp. 21859–21865, Sep. 2014.

[77] A. Rahim *et al.*, "Expanding the silicon photonics portfolio with silicon nitride photonic integrated circuits," *J. Lightw. Technol.*, vol. 35, no. 4, pp. 639–649, Feb. 2017.

[78] J. W. Choi, G. F. Chen, D. K. Ng, K. J. Ooi, and D. T. Tan, "Wideband nonlinear spectral broadening in ultra-short ultra - silicon rich nitride waveguides," *Sci. Rep.*, vol. 6, no. 1, Jun. 2016, Art. no. 27120.

[79] T. Wang *et al.*, "Supercontinuum generation in bandgap engineered, back-end CMOS compatible silicon rich nitride waveguides," *Laser Photon. Rev.*, vol. 9, no. 5, pp. 498–506, Aug. 2015.

[80] Y. Wang *et al.*, "Amorphous silicon-lithium niobate thin film strip-loaded waveguides," *Opt. Mater. Express*, vol. 7, no. 11, pp. 4018–4028, Nov. 2017.

[81] J. Chiles *et al.*, "Low-loss, submicron chalcogenide integrated photonics with chlorine plasma etching," *Appl. Phys. Lett.*, vol. 106, no. 11, Mar. 2015, Art. no. 111110.

[82] Q. Du *et al.*, "Low-loss photonic device in Ge–Sb–S chalcogenide glass," *Opt. Lett.*, vol. 41, no. 13, pp. 3090–3093, Jul. 2016.

[83] J. E. Tremblay *et al.*, "High-q and low-loss chalcogenide waveguide for nonlinear supercontinuum generation," in *Proc. IEEE Photon. Conf.*, 2016, pp. 158–159.

[84] L. Li *et al.*, "Integrated flexible chalcogenide glass photonic devices," *Nature Photon.*, vol. 8, no. 8, pp. 643–649, Aug. 2014.

[85] S. F. Serna Otálvaro *et al.*, "Third order nonlinear properties of GeSbS chalcogenide waveguides," in *Proc. Conf. Frontiers Opt.*, 2017, Paper JW3A.72.

[86] P. Rabiei, J. Ma, J. Chiles, S. Khan, and S. Fathpour, "Submicron optical waveguides and microring resonators fabricated by selective oxidation of tantalum," *Opt. Express*, vol. 21, no. 6, pp. 6967–6972, Mar. 2013.

[87] P. Rabiei, A. Rao, J. Chiles, J. Ma, and S. Fathpour, "Low-loss and high index-contrast tantalum pentoxide microring resonators and grating couplers on silicon substrates," *Opt. Lett.*, vol. 39, no. 18, pp. 5379–5382, Sep. 2014.

[88] S. Li, L. Cai, Y. Wang, Y. Jiang, and H. Hu, "Waveguides consisting of single-crystal lithium niobate thin film and oxidized titanium stripe," *Opt. Express*, vol. 23, no. 19, pp. 24212–24219, Sep. 2015.

[89] A. Klenner *et al.*, "Gigahertz frequency comb offset stabilization based on supercontinuum generation in silicon nitride waveguides," *Opt. Express*, vol. 24, pp. 11043–11053, 2016.

[90] V. Brasch *et al.*, "Photonic chip-based optical frequency comb using soliton Cherenkov radiation," *Science*, vol. 351, no. 6271, pp. 357–360, Jan. 2016.

[91] L. Chen, J. Nagy, and R. M. Reano, "Patterned ion-sliced lithium niobate for hybrid photonic integration on silicon," *Opt. Mater. Express*, vol. 6, no. 7, pp. 2460–2467, Jul. 2016.

[92] P. O. Weigel *et al.*, "Lightwave circuits in lithium niobate through hybrid waveguides with silicon photonics," *Sci. Rep.*, vol. 6, Mar. 2016, Art. no. 22301.

[93] L. Cai, R. Kong, Y. Wang, and H. Hu, "Channel waveguides and y-junctions in x-cut single-crystal lithium niobate thin film," *Opt. Express*, vol. 23, no. 22, pp. 29211–29221, Nov. 2015.

[94] C. Wang, M. Zhang, B. Stern, M. Lipson, and M. Lončar, "Nanophotonic lithium niobate electro-optic modulators," *Opt. Express*, vol. 26, no. 2, pp. 1547–1555, Jan. 2018.

[95] D. Dofli and T. R. Ranganath, "50 GHz velocity-matched, broad wavelength $LiNbO_3$ modulator with multimode active section," *Electron. Lett.*, vol. 28, no. 13, pp. 1197–1198, Jun. 1992.

[96] J. Kondo *et al.*, "40-Gb/s X-Cut $LiNbO_3$ optical modulator with two-step back-slot structure," *J. Lightw. Technol.*, vol. 20, no. 12, pp. 2110–2114, Dec. 2002.

[97] M. M. Howerton, R. P. Moeller, A. S. Greenblatt, and R. Krahenbuhl, "Fully packaged, broad-band $LiNbO_3$ modulator with low drive voltage," *IEEE Photon. Technol. Lett.*, vol. 12, no. 7, pp. 792–794, Jul. 2000.

[98] C. Cox, E. Ackerman, G. Betts, and J. Prince, "Limits on the performance of RF-over-fiber links and their impact on device design," *IEEE Trans. Microw. Theory Techn.*, vol. 54, no. 2, pp. 906–920, Feb. 2006.

[99] C. Wang *et al.*, "Second harmonic generation in nano-structured thin-film lithium niobate waveguides," *Opt. Express*, vol. 25, no. 6, pp. 6963–6973, Mar. 2017.

[100] L. Cai, Y. Wang, and H. Hu, "Efficient second harmonic generation in $\chi^{(2)}$ profile reconfigured lithium niobate thin film," *Opt. Commun.*, vol. 387, pp. 405–408, Mar. 2017.

[101] R. Luo *et al.*, "On-chip second-harmonic generation and broadband parametric down-conversion in a lithium niobate microresonator," *Opt. Express*, vol. 25, no. 20, pp. 24531–24539, Oct. 2017.

[102] R. Wolf, I. Breunig, H. Zappe, and K. Buse, "Cascaded second-order optical nonlinearities in on-chip micro rings," *Opt. Express*, vol. 25, no. 24, pp. 29927–29933, Nov. 2017.

[103] C. Wang *et al.*, "Metasurface-assisted phase-matching-free second harmonic generation in lithium niobate waveguides," *Nature Commun.*, vol. 8, Dec. 2017, Art. no. 2098.

[104] K. R. Parameswaran, J. R. Kurz, R. V. Roussev, and M. M. Fejer, "Observation of 99% pump depletion in single-pass second-harmonic generation in a periodically poled lithium niobate waveguide," *Opt. Lett.*, vol. 27, no. 1, pp. 43–45, Jan. 2002.

[105] M. M. Fejer, G. A. Magel, D. H. Jundt, and R. L. Byer, "Quasi-phase-matched second harmonic generation: Tuning and tolerances," *IEEE J. Quantum Electron.*, vol. 28, no. 11, pp. 2631–2654, Nov. 1992.

[106] M. Davanco *et al.*, "Heterogeneous integration for on-chip quantum photonic circuits with single quantum dot devices," *Nature Commun.*, vol. 8, Oct. 2017, Art. no. 889.

[107] I. Sawaki, H. Nakajima, M. Seino, and K. Asama, "Thermally stabilized z-cut Ti:$LiNbO_3$ waveguide switch," in *Proc. Tech. Dig. Conf. Lasers Electroopt.*, 1986, pp. 46–47.

[108] M. Seino *et al.*, "A low DC-drift Ti:$LiNbO_3$ modulator assured over 15 years," in *Proc. Dig. Conf. Opt. Fiber Commun.*, San Jose, CA, USA, 1992, pp. 325–328.

[109] H. Nagata, "DC drift failure rate estimation on 10 Gb/s X-cut lithium niobate modulators," *IEEE Photon. Technol. Lett.*, vol. 12, no. 11, pp. 1477–1479, Nov. 2000.

[110] D. A. B. Miller, "Device requirements for optical interconnects to silicon chips," *Proc. IEEE*, vol. 97, no. 7, pp. 1166–1185, Jul. 2009.

[111] R. DeSalvo *et al.*, "The convergence of microwave photonic and optical wireless systems with military communication and sensor systems," in *Proc. Avionics Veh. Fiber-Opt. Photon. Conf.*, 2016, pp. 191–192.

[112] A. Paolella, "Hybrid integration of RF photonic systems," in *Proc. Avionics Veh. Fiber-Opt. Photon. Conf.*, 2017 pp. 29–30.

[113] C. Schuetz, "Optical techniques for millimeter-wave detection and imaging," Ph.D. dissertation, Univ. Delaware, Newark, DE, USA, 2007.

[114] L. Chen, and R. M. Reano, "Compact electric field sensors based on indirect bonding of lithium niobate to silicon microrings," *Opt. Express*, vol. 20, no. 4, pp. 4032–4038, Feb. 2012.

[115] D. Carlson *et al.*, "Photonic-chip supercontinuum with tailored spectra for precision frequency metrology," *Phys. Rev. Appl.*, vol. 8, 2017, Art. no. 014027.

[116] S. Khan *et al.*, "Integrated thin-film lithium-niobate waveguides on silicon for second-harmonic generation pumped at 1875 nm," in *Proc. Conf. Lasers Electro-Opt.*, 2018, Paper STu3F.4.

[117] N. Nader *et al.*, "Versatile silicon-waveguide supercontinuum for coherent mid-infrared spectroscopy," *APL Photon.*, vol. 3, 2017, Art. no. 036102.

[118] A. Rao *et al.*, "Photon pair generation on a silicon chip using nanophotonic periodically-poled lithium niobate waveguides," in *Proc. Conf. Lasers Electro-Opt.*, 2018, Paper JTh3C.2.

[119] A. Rao *et al.*, "Spectral resolution of second-order coherence of broadband biphotons," in *Proc. Conf. Lasers Electro-Opt.*, 2018, Paper JTh2A.16.

[120] D. D. Hickstein *et al.*, "High-harmonic generation in periodically poled waveguides," *Optica*, vol. 4, no. 12, pp. 1538–1544, Dec. 2017.

[121] A. Rao *et al.*, "Random quasi-phase-matching on a nanophotonic heterogeneous silicon chip," in *Proc. Conf. Lasers Electro-Opt.*, 2018, Paper SM1B.2.

[122] X. Ji *et al.*, "Ultra-low-loss on-chip resonators with sub-milliwatt parametric oscillation threshold," *Optica*, vol. 4, no. 6, pp. 619–624, Jun. 2017.

[123] H. Liang, R. Luo, Y. He, H. Jiang, and Q. Lin, "High-quality lithium niobate photonic crystal nanocavities," *Optica*, vol. 4, no. 10, pp. 1251–1258, Oct. 2017.

[124] H. Jiang *et al.*, "Fast response of photorefraction in lithium niobate microresonators," *Opt. Lett.*, vol. 42, no. 17, pp. 3267–3270, Sep. 2017.

[125] X. Sun *et al.*, "Nonlinear optical oscillation dynamics in high-Q lithium niobate microresonators," *Opt. Express*, vol. 25, no. 12, pp. 13504–13516, Jun. 2017.

[126] R. Luo, H. Jiang, H. Liang, Y. Chen, and Q. Lin, "Self-referenced temperature sensing with a lithium niobate microdisk resonator," *Opt. Lett.*, vol. 42, no. 7, pp. 1281–1284, Apr. 2017.

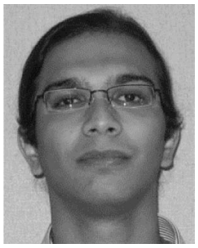

Ashutosh Rao (S'16) received the B.Tech. and M.Tech. degrees in engineering physics from the Indian Institute of Technology Bombay, Mumbai, India, in 2013. He received the Ph.D. degree in optics and laser engineering from CREOL, The College of Optics and Photonics, University of Central Florida, Orlando, FL, USA, in 2018.

His research has included demonstrations of high-speed electrooptic modulators, second-order nonlinear optical frequency converters, and photon-pair generation in thin-film lithium niobate waveguides. His current research interests include chip-scale quantum-state engineering and integrated photonics, and he is a co-author of about 30 journal and conference papers.

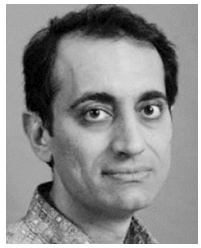

Sasan Fathpour (S'01–M'04–SM'13) received the Ph.D. degree in electrical engineering from the University of Michigan, Ann Arbor, MI, USA, in 2005. He is currently an Associate Professor at CREOL, The College of Optics and Photonics, University of Central Florida. He joined the Electrical Engineering Department, University of California, Los Angeles (UCLA) as a Postdoctoral Fellow and joined the CREOL faculty in 2008. His current research interests include heterogeneous integrated photonics, nonlinear integrated optics, silicon photonics, and nonconventional optical waveguide platforms for mid-wave infrared and other applications.

Prof. Fathpour is a recipient of the ONR Young Investigator Award (2013) and the NSF CAREER Award (2012). He is the coeditor of a book entitled "*Silicon Photonics for Telecommunications and Biomedicine*," published by CRC Press in 2012, and a coauthor of over 150 journal and conference papers, book chapters and patents. He is a Fellow of OSA, the Optical Society, and a Senior Member of SPIE.